Effects of Intermolecular Vibrational Coupling and Liquid Dynamics on the Polarized Raman and Two-Dimensional Infrared Spectral Profiles of Liquid *N,N*-Dimethylformamide Analyzed with a Time-Domain Computational Method

Hajime Torii*

Department of Chemistry, School of Education, Shizuoka University, 836 Ohya, Shizuoka 422-8529, Japan

Received: January 2, 2006; In Final Form: February 21, 2006

A time-domain method for calculating polarized Raman and two-dimensional infrared (2D-IR) spectra that includes the effects of both the diagonal frequency modulations (of individual molecules in the system) and the off-diagonal (intermolecular) vibrational coupling is presented and applied to the case of the amide I band of liquid *N,N*-dimethylformamide. It is shown that the effect of the resonant off-diagonal vibrational coupling and the resulting delocalization of vibrational modes is clearly seen as the noncoincidence effect in the polarized Raman spectrum and some spectral features (especially as asymmetric intensity patterns) in the 2D-IR spectra. The type of 2D-IR spectra (concerning the polarization condition) most appropriate for observing this effect is discussed. On the basis of the agreement between the observed and calculated band profiles of the polarized Raman spectrum, the time dependence of the transient IR absorption anisotropy is also calculated. The method of evaluating the extent of delocalization of vibrational modes that is relevant to the features of these optical signals in the time and frequency domains is discussed. The nature of the molecular motions (concerning the liquid dynamics) that are effective on the diagonal frequency modulations is also examined.

1. Introduction

To understand the vibrational spectra of liquid-phase systems in a quantitative way, it is important to correctly consider the effects of surrounding molecules. Such effects are classified into two types.[1] One is the diagonal effect, which is the local environmental effect on the vibrations of individual molecules. This effect is present both in concentrated liquids (including neat liquids) and in dilute solutions, and in the latter case, it is generally regarded as a "solvent effect". In principle, it is possible to represent this effect with fields on the locations where the individual molecules are present. For the vibrational modes having sufficiently large dipole derivatives and mechanical (and electrical) anharmonicities, the vibrational frequencies of individual molecules are controlled by the electric fields from the surrounding molecules.[2−9] The other is the off-diagonal effect, which is the direct vibrational coupling between molecules. This effect is called off-diagonal, since it is represented by the off-diagonal terms of the vibrational Hamiltonian of the coupled-oscillator systems. This direct vibrational coupling gives rise to spatial delocalization of vibrational modes in the resonant case, where the intrinsic frequencies of the interacting vibrational modes are sufficiently close to each other as compared with the magnitude of the coupling. The effect of this delocalization is clearly seen in the frequency domain as the noncoincidence effect (NCE),[9−27] which is the phenomenon that the isotropic and anisotropic components of the Raman band and the infrared (IR) band of the same vibrational mode appear at different frequency positions. The NCE of significant magnitude is seen for many vibrational modes with large dipole derivatives, for which the vibrational coupling is caused by the transition dipole coupling (TDC) mechanism.[1,19−21] The fact that the NCE of such modes arises from the resonant off-diagonal vibrational coupling is supported by the isotopic and chemical dilution experiments,[22−27] in which the magnitude of the NCE decreases as the coupled molecules become separated from each other upon dilution. It should be noted at this point that similar spectral features are also seen in the spectra of polypeptides and proteins,[28−46] where some vibrational modes of peptide groups (such as the amide I mode) are strongly coupled.

The development of ultrafast IR lasers has enabled measurements of the effect of resonant off-diagonal vibrational coupling also in the time domain as the ultrafast decay of transient IR absorption anisotropy.[47,48] This may be regarded as a time-domain counterpart to the NCE in the frequency domain.[1,49] Because of the off-diagonal vibrational coupling, the vibrational excitations initially made by the first IR laser pulse migrate to other molecules as time evolves, and the IR excitations become progressively depolarized if those molecules are oriented in different directions. The decay on the order of 70 fs has been observed for the OH stretching mode of liquid water (neat liquid H_2O).[47,48]

The development of ultrafast IR lasers has also made possible the progress of two-dimensional infrared (2D-IR) spectroscopy.[34,50−55] 2D-IR band profiles are considered to be sensitive to the anharmonicities and the off-diagonal vibrational coupling,[34,35,53−57] meaning that information on the structures and dynamics (i.e., distances and orientations of the groups involved in the vibrational coupling and their time evolution) is contained in those 2D-IR band profiles. Experimental and theoretical studies have been performed to characterize the 2D-IR band profiles related to the structures and interactions in condensed-phase systems.[34−36,50−66]

In previous theoretical studies on the 2D-IR spectra of coupled molecular systems (liquids and peptides),[35,56−59] the calculations have been carried out by transforming the formulas to those in the frequency domain (the sum-over-states picture). However, the diagonal frequencies of individual molecules and the off-diagonal vibrational coupling terms are both modulated by liquid

* Phone and Fax: +81-54-238-4624. E-mail: torii@ed.shizuoka.ac.jp.

10.1021/jp060014c CCC: $33.50
Published on Web 03/21/2006

dynamics, so that the vibrational Hamiltonian is time dependent. Those modulations are often in the fast modulation regime in the liquid phase, to the extent that the effect of the modulations is noticeable in the vibrational band profiles.[9] It is therefore necessary to develop a time-domain method for calculating vibrational spectra (including 2D-IR spectra) of coupled oscillator systems controlled by the time-dependent vibrational Hamiltonian to correctly analyze those band profiles. The development of such a time-domain method is especially helpful to consider how we can evaluate the extent of delocalization of vibrational modes that influence the band profiles. Usually, the extent of delocalization of vibrational modes is evaluated by calculating the participation ratio[67−70] on the basis of the instantaneous normal mode picture (i.e., in the frequency domain). However, it is necessary to examine how meaningful this quantity is in the presence of the fast modulations of the vibrational Hamiltonian.

In the present study, a time-domain method for calculating 2D-IR spectra that includes the effects of both the diagonal frequency modulations and the off-diagonal vibrational coupling is developed[71] as an extension of the same type of method for polarized Raman spectra,[9] and is applied to the amide I band of liquid *N*,*N*-dimethylformamide (DMF). To see the validity of the parameters and to form the basis for analyzing the 2D-IR spectra, the polarized Raman spectrum is calculated and compared with the observed spectrum. In addition to the problem on the method of evaluating the extent of delocalization, we examine what kind of molecular motions (concerning the liquid dynamics) are effective on the frequency modulations. The type of 2D-IR spectra (concerning the polarization condition) most appropriate for observing the effect of delocalization of vibrational modes is also discussed.

2. Theoretical Formulation

The time-domain method for calculating polarized Raman spectra developed previously[9] is briefly described as follows. The wave function of the Raman excitation at time t related to the pq element of the polarizability operator α_{pq} (where $p, q = 1, 2, 3$ corresponds to the x, y, and z axes of the system) is expressed as

$$|\psi_{pq}^{(\mathrm{R})}(t,t_0)\rangle = \exp_+\left[-\frac{i}{\hbar}\int_{t_0}^{t} \mathrm{d}\tau H^{1\mathrm{Q}}(\tau)\right]|\psi_{pq}^{(\mathrm{R})}(t_0,t_0)\rangle \quad (1)$$

where

$$|\psi_{pq}^{(\mathrm{R})}(t_0,t_0)\rangle = \sum_{m=1}^{N} |m\rangle \langle m|\alpha_{pq}(t_0)|0\rangle \quad (2)$$

is the wave function initially made by the Raman excitation at time t_0, expressed by the wave functions of the ground state $|0\rangle$ and the one-quantum ($v = 1$) excited state $|m\rangle$ on the mth molecule ($1 \le m \le N$), and the polarizability operator $\alpha_{pq}(t_0)$ evaluated with the molecular orientations at time t_0. $H^{1\mathrm{Q}}(\tau)$ is the vibrational Hamiltonian for the one-quantum excited states (defined below), whose diagonal and off-diagonal terms are both dependent on the liquid structures and is therefore time-dependent because of the liquid dynamics, which is calculated by the molecular dynamics (MD) method in the present scheme. N is the number of molecules participating in the vibrational band in question, so that $|\psi_{pq}^{(\mathrm{R})}(t,t_0)\rangle$ and $H^{1\mathrm{Q}}(\tau)$ are represented by an N-dimensional vector and an $N \times N$ matrix, respectively.

The time-ordered exponential (denoted as $\exp_+$)[72] in eq 1 is evaluated as the product of short-time evolutions assuming that the Hamiltonian is essentially invariant during a very short time period $\Delta\tau$, which is taken as equal to the time step of the MD simulations. We obtain[9,73]

$$|\psi_{pq}^{(\mathrm{R})}(\tau+\Delta\tau,t_0)\rangle = \exp\left[-\frac{i}{\hbar}\Delta\tau\, H^{1\mathrm{Q}}(\tau)\right]|\psi_{pq}^{(\mathrm{R})}(\tau,t_0)\rangle = \sum_{\xi=1}^{N} |\xi_\tau'\rangle \exp[-i\omega_\xi(\tau)\Delta\tau]\langle\xi_\tau|\psi_{pq}^{(\mathrm{R})}(\tau,t_0)\rangle \quad (3)$$

where $\omega_\xi(\tau)$ is the vibrational frequency for the eigenstate $|\xi_\tau\rangle$ (numbered by ξ) of $H^{1\mathrm{Q}}(\tau)$, and $|\xi_\tau'\rangle$ is the wave function with the same amplitudes of molecular vibrations as $|\xi_\tau\rangle$ but with the molecular orientations evaluated at time $\tau + \Delta\tau$.

Assuming $\hbar\omega \gg kT$, the Raman spectrum $I_{pq}^{(\mathrm{R})}(\omega)$ is expressed as

$$I_{pq}^{(\mathrm{R})}(\omega) = \mathrm{Re}\int_0^\infty \mathrm{d}t \exp(i\omega t)\left\langle\langle 0|\alpha_{pq}(t)|\psi_{pq}^{(\mathrm{R})}(t,0)\rangle\right\rangle \quad (4)$$

where the large bracket stands for statistical average, assuming that the effect of vibrational population relaxation is negligible. The isotropic and anisotropic components of the Raman spectrum are obtained from appropriate combinations of $I_{pq}^{(\mathrm{R})}(\omega)$ with $p, q = 1, 2, 3$. In the same way, the (one-dimensional) IR spectrum $I_p^{(\mathrm{IR})}(\omega)$ is expressed as

$$I_p^{(\mathrm{IR})}(\omega) = \mathrm{Re}\int_0^\infty \mathrm{d}t \exp(i\omega t)\left\langle\langle 0|\mu_p(t)|\psi_p^{(\mathrm{IR})}(t,0)\rangle\right\rangle \quad (5)$$

where $\mu_p(t)$ is the dipole operator evaluated with the molecular orientations at time t, and $|\psi_p^{(\mathrm{IR})}(t,t_0)\rangle$ is the wave function of the IR excitation at time t, expressed as

$$|\psi_p^{(\mathrm{IR})}(t,t_0)\rangle = \exp_+\left[-\frac{i}{\hbar}\int_{t_0}^{t}\mathrm{d}\tau\, H^{1\mathrm{Q}}(\tau)\right]|\psi_p^{(\mathrm{IR})}(t_0,t_0)\rangle \quad (6)$$

where

$$|\psi_p^{(\mathrm{IR})}(t_0,t_0)\rangle = \sum_{m=1}^{N} |m\rangle\langle m|\mu_p(t_0)|0\rangle \quad (7)$$

is the wave function initially made by the IR excitation at time t_0.

In the present study, this method is extended to calculate 2D-IR spectra. The diagrams involved in the optical processes of 2D-IR spectra considered in the present study are shown in Figure 1. The signals in the direction of $\boldsymbol{k}_S = -\boldsymbol{k}_1 + \boldsymbol{k}_2 + \boldsymbol{k}_3$ are considered, where $\boldsymbol{k}_i$ ($i = 1, 2, 3$) is the wave vector of the input laser pulses. It is supposed that the second and third pulses interact simultaneously with the system after time t_1 (≥ 0) from the first pulse, and the signals ($\boldsymbol{k}_S$) after time t_3 (≥ 0) are detected. Some of these optical processes contain two-quantum excited states, but only the coherences of the one-quantum transition frequencies (between $v = n$ and $n \pm 1$) are formed during t_1 and t_3. For the first three diagrams (R_1-R_3, called type I hereafter), the pulse of $\boldsymbol{k}_1$ arrives earlier than that of $\boldsymbol{k}_2$ and $\boldsymbol{k}_3$, so that the coherences in the t_1 and t_3 time periods are rephasing.[54−57,62] (There are an additional three diagrams obtained by interchanging $\boldsymbol{k}_2$ and $\boldsymbol{k}_3$.) For the other five diagrams (R_4-R_8, called type II hereafter) the pulse of $\boldsymbol{k}_2$ arrives earlier than that of $\boldsymbol{k}_1$ and $\boldsymbol{k}_3$, so that the coherences in the t_1 and t_3 time periods are nonrephasing.

The 2D-IR spectrum for the type I processes (R_1-R_3) is calculated as the double Fourier transform of $S^{(1)}(t_3,t_1) + S^{(2)}(t_3,t_1) - S^{(3)}(t_3,t_1)$, where each $S^{(j)}(t_3,t_1)$ is the time correlation

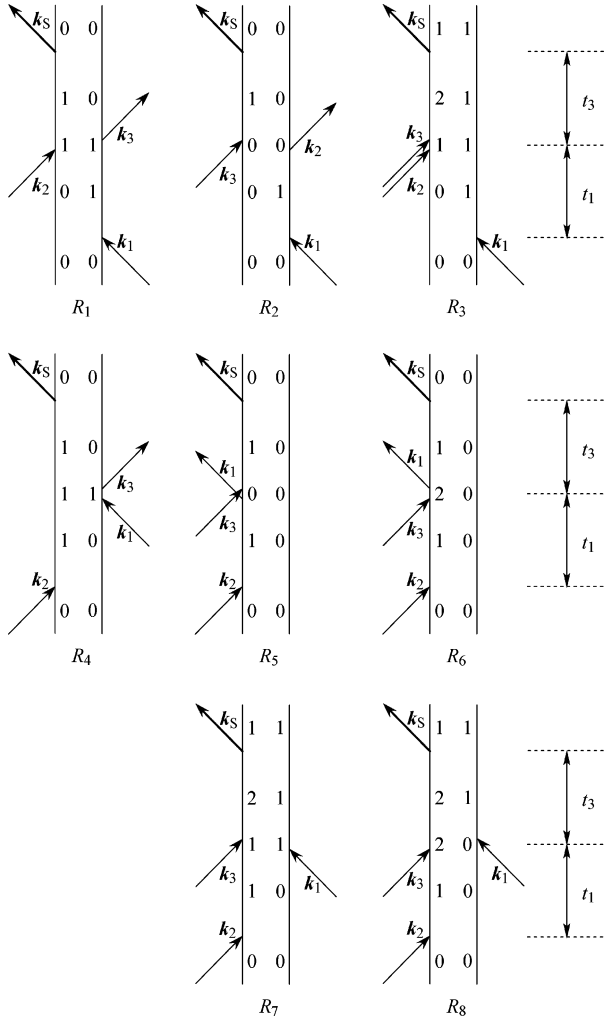

Figure 1. Diagrams of the type I (R_1-R_3, rephasing) and type II (R_4-R_8, nonrephasing) optical processes involved in 2D-IR spectra. The number of vibrational quanta on the bra and ket sides is indicated in the middle column of each diagram.

function corresponding to the diagram R_j, expressed as

$$S^{(1)}_{srqp}(t_3,t_1) = S^{(2)}_{sqrp}(t_3,t_1) = \left\langle \langle 0|\mu_s(t_1+t_3)|\psi^{(\mathrm{IR})}_r(t_1+t_3,t_1)\rangle \langle 0|\mu_q(t_1)|\psi^{(\mathrm{IR})}_p(t_1,0)\rangle^* \right\rangle \quad (8)$$

$$S^{(3)}_{srqp}(t_3,t_1) = \left\langle \sum_{m=1}^{N} \left\langle m\right|^{\mathrm{T}} U_s(t_1+t_3)\, \exp_+\left[-\frac{i}{\hbar}\int_{t_1}^{t_1+t_3} \mathrm{d}\tau \times H^{2\mathrm{Q}}(\tau)\right] U_r(t_1)\mu_q(t_1)\left|0\right\rangle \langle m|\psi^{(\mathrm{IR})}_p(t_1+t_3,0)\rangle^* \right\rangle \quad (9)$$

where $H^{2Q}(\tau)$ is the vibrational Hamiltonian of the two-quantum excited states, $\boldsymbol{U}(\tau)$ is the transition operator between the one-quantum and two-quantum excited states, and the superscript T stands for the transpose of the matrix. Note that to evaluate the time-ordered exponential in eq 9 in the same way as shown in eq 3, the eigenstates of $H^{2Q}(\tau)$ [of dimension equal to $N(N+1)/2$] should be calculated at every time step $\Delta\tau$. The 2D-IR spectrum for the type II processes (R_4-R_8) is calculated as the double Fourier transform of $S^{(4)}(t_3,t_1) + S^{(5)}(t_3,t_1) + S^{(6)}(t_3,t_1) - S^{(7)}(t_3,t_1) - S^{(8)}(t_3,t_1)$, where

$$S^{(4)}_{srqp}(t_3,t_1) = \left\langle \langle 0|^{\mathrm{T}}\mu_s(t_1+t_3)|\psi^{(\mathrm{IR})}_q(t_1+t_3,0)\rangle \langle 0|^{\mathrm{T}}\mu_r(t_1)\mu_p(t_1)|0\rangle^* \right\rangle \quad (10)$$

$$S^{(5)}_{srqp}(t_3,t_1) = \left\langle \langle 0|^{\mathrm{T}}\mu_s(t_1+t_3)|\psi^{(\mathrm{IR})}_r(t_1+t_3,t_1)\rangle \langle 0|^{\mathrm{T}}\mu_p(t_1)|\psi^{(\mathrm{IR})}_q(t_1,0)\rangle \right\rangle \quad (11)$$

$$S^{(6)}_{srqp}(t_3,t_1) = \left\langle\left\langle 0\right|^{\mathrm{T}}\mu_s(t_1+t_3) \times \exp_+\left[-\frac{i}{\hbar}\int_{t_1}^{t_1+t_3} \mathrm{d}\tau\, H^{1\mathrm{Q}}(\tau)\right]^{\mathrm{T}} U_p(t_1)U_r(t_1)\left|\psi^{(\mathrm{IR})}_q(t_1,0)\right\rangle\right\rangle \quad (12)$$

$$S^{(7)}_{srqp}(t_3,t_1) = S^{(8)}_{srqp}(t_3,t_1) = \left\langle \sum_{m=1}^{N} \left\langle m\right|^{\mathrm{T}} U_s(t_1+t_3) \times \exp_+\left[-\frac{i}{\hbar}\int_{t_1}^{t_1+t_3} \mathrm{d}\tau\, H^{2\mathrm{Q}}(\tau)\right] U_r(t_1)\left|\psi^{(\mathrm{IR})}_q(t_1,0)\right\rangle \times \langle m|\psi^{(\mathrm{IR})}_p(t_1+t_3,t_1)\rangle^* \right\rangle \quad (13)$$

The "absorptive" 2D-IR spectrum is calculated as the sum of the spectra of the type I (with inversion of the sign of ω_1) and type II processes.

In the computational scheme of the present study, the vibrational Hamiltonians are constructed in the following way, from the liquid structures and dynamics obtained in the MD simulations. The modulations in the diagonal terms of H^{1Q} (the shift from $\hbar\sqrt{k_m}$) due to the effect of the electric field from the surrounding molecules are expressed as[9,74−76]

$$\Delta H^{1\mathrm{Q}}_{mm} = \frac{\hbar}{2\sqrt{k_m}}\left(\frac{f_m}{k_m}\frac{\partial \boldsymbol{\mu}_m}{\partial q_m} - \frac{\partial^2 \boldsymbol{\mu}_m}{\partial {q_m}^2}\right)\boldsymbol{E}_m \quad (14)$$

where k_m and f_m are the diagonal quadratic and cubic force constants for the vibration of the mth molecule (q_m), and $\boldsymbol{E}_m$ is the electric field operating on the mth molecule from the surrounding molecules. The modulations in the diagonal terms of H^{2Q} are given as

$$\Delta H^{2\mathrm{Q}}_{m+n,m+n} = \Delta H^{1\mathrm{Q}}_{mm} + \Delta H^{1\mathrm{Q}}_{nn} - \delta_{mn}\frac{5\hbar^2}{24}\left(\frac{f_m}{k_m}\right)^2 \quad (15)$$

where "$m + n$" in the subscript stands for the state with one quantum each on the mth and nth molecules ($m \neq n$, called "combination state") or with two quanta on the mth molecule ($m = n$, called "overtone state"). The third term is effective only for the latter type of states and represents the effect of mechanical anharmonicity on the energy levels of the two-quantum excited states.

The off-diagonal terms of H^{1Q} are determined by the transition dipole coupling (TDC) mechanism,[9,20,21,29,31] expressed as

$$H^{1\mathrm{Q}}_{mn} = -\frac{\hbar}{2(k_m k_n)^{1/4}}\frac{\partial \boldsymbol{\mu}_m}{\partial q_m}\boldsymbol{T}_{mn}\frac{\partial \boldsymbol{\mu}_n}{\partial q_n} \qquad (m \neq n) \quad (16)$$

where $\boldsymbol{T}_{mn}$ is the dipole interaction tensor between the mth and nth molecules, which is given as

$$\boldsymbol{T}_{mn} = \frac{3\boldsymbol{r}_{mn}\boldsymbol{r}_{mn} - {r_{mn}}^2\boldsymbol{I}}{{r_{mn}}^5} \quad (17)$$

where $\boldsymbol{r}_{mn} = \boldsymbol{r}_m - \boldsymbol{r}_n$ is the distance vector (of length r_{mn}) between the two molecules, and $\boldsymbol{I}$ is a 3×3 unit tensor. The off-diagonal terms of H^{2Q} are evaluated in the harmonic approximation as

$$\frac{1}{\sqrt{2}}H^{2Q}_{l+m,m+m} = H^{2Q}_{l+n,m+n} = H^{1Q}_{lm} \qquad (l \neq m,\ l \neq n,\ m \neq n) \tag{18}$$

The transition operator $\boldsymbol{U}$ between the one-quantum and two-quantum excited states is also calculated in the harmonic approximation, and is given as

$$\frac{1}{\sqrt{2}}\langle m+m|\boldsymbol{U}|m\rangle = \langle l+m|\boldsymbol{U}|l\rangle = \langle m|\boldsymbol{\mu}|0\rangle \qquad (l \neq m) \tag{19}$$

The time dependence of the transient IR absorption anisotropy is calculated by combining $|\psi_p^{(IR)}(t,t_0)\rangle$ in eq 6 with the formulas described in our previous study.[49] The transient IR absorption intensity at delay time t from the pump pulse is expressed as

$$D_{qp}(t) = \left\langle \sum_{\lambda=1}^{N} |\langle \lambda_t^{ov}|U_q(t)|\psi_p^{(IR)}(t,0)\rangle|^2 \right\rangle \tag{20}$$

where $|\lambda_t^{ov}\rangle$ is an eigenstate (numbered by λ) in the overtone band at time t. By using eq 19, and assuming that the overtone band is spectrally separated from the combination band, we have

$$D_{qp}(t) \cong \left\langle \sum_{m=1}^{N} 2\ |\langle m|\mu_q(t)|0\rangle|^2 |\langle m|\psi_p^{(IR)}(t,0)\rangle|^2 \right\rangle \tag{21}$$

The anisotropy of the transient absorption is then given as

$$A(t) = \frac{D_{||}(t) - D_{\perp}(t)}{D_{||}(t) + 2D_{\perp}(t)} \tag{22}$$

with

$$D_{||}(t) = D_{pp}(t) \tag{23}$$

$$D_{\perp}(t) = \frac{1}{2}\sum_{q(\neq p)} D_{qp}(t) \tag{24}$$

3. Computational Procedure

The parameters of molecular properties needed for constructing the vibrational Hamiltonians were determined as follows. The value of k_m was assumed to be $6.1060 \times 10^{-5} E_h a_0^{-2} m_e^{-1}$ (=1.7329 mdyn Å^{-1} amu^{-1}), which corresponds to the vibrational frequency 1715 cm^{-1} in the gas phase.[77,78] The ratio $f_m/k_m = -2.11 \times 10^{-2} a_0^{-1} m_e^{-1/2}$ was taken from the result of the ab initio molecular orbital (MO) calculation (by using Gaussian 03[79]) for an isolated DMF molecule at the MP3/6-31+G(2d,p) level. At the same theoretical level, the dipole first and second derivatives were calculated as $|\partial\boldsymbol{\mu}_m/\partial q_m| = (1.8125 \times 10^{-2}) e m_e^{-1/2}$ and $|\partial^2\boldsymbol{\mu}_m/\partial {q_m}^2| = (5.2511 \times 10^{-5}) e a_0^{-1} m_e^{-1}$ in magnitude, being tilted by 24.1° and 187.4°, respectively, from the $\boldsymbol{r}_{CO}$ ($\equiv \boldsymbol{r}_C - \boldsymbol{r}_O$) direction toward the $\boldsymbol{r}_{NC}$ direction. By using these values of $|\partial\boldsymbol{\mu}_m/\partial q_m|$ and $|\partial^2\boldsymbol{\mu}_m/\partial {q_m}^2|$, however, it was found that the vibrational frequency shift and the magnitude of the NCE (related to these derivatives as shown in eqs 14 and 16) were calculated to be a little too large. We therefore reduced the magnitudes to 85% of these values ($1.5407 \times 10^{-2} e m_e^{-1/2}$ and $4.4635 \times 10^{-5} e a_0^{-1} m_e^{-1}$). The good agreement between the observed and calculated polarized Raman spectral features (discussed below) suggests that these reduced values constitute a reasonable set of molecular parameters. In constructing the vibrational Hamiltonian, the interaction point of these derivatives was assumed to be located at the center of the C=O bond of each molecule. To calculate the polarized Raman spectrum, the polarizability derivative $\partial\boldsymbol{\alpha}_m/\partial q_m$ was also needed. By referring to the result of the calculation at the MP3/6-31+G(2d,p) level, it was assumed to be axially symmetric with the principal axis tilted by 29.8° from the $\boldsymbol{r}_{CO}$ direction toward the $\boldsymbol{r}_{NC}$ direction.

To calculate the electric field $\boldsymbol{E}_m$ in eq 14 and to perform MD simulations of the liquid structures and dynamics, the CH and CH_3 groups in DMF were modeled as united atoms. The partial charges of the five interaction points [q(CH) = 0.505e, q(O) = −0.553e, q(N) = −0.317e, q(CH_3, trans to O) = 0.165e, and q(CH_3, cis to O) = 0.200e] were determined by fitting to the electrostatic potential around an isolated DMF molecule calculated at the MP3/6-31+G(2d,p) level according to the scheme shown in our previous study.[76]

The MD simulation for calculating the IR and polarized Raman spectra and the time dependence of the transient IR absorption anisotropy was performed for the liquid system of 128 molecules in a cubic cell, by using the above atomic charges combined with the Lennard-Jones parameters taken from ref 80. The volume of the cubic cell was fixed so that the molecular volume was equal to v = 128.6 Å^3, which corresponds to the density of 0.944 g cm^{-3}.[81] The temperature was kept at 298.15 K. The time step $\Delta\tau$ was set to 2 fs. To obtain a frequency resolution of ∼0.5 cm^{-1} for the calculated spectra, the time evolution of $|\psi_{pq}^{(R)}(t,t_0)\rangle$ was calculated for about 65.5 ps (32 768 time steps). The calculations were carried out for 1350 samples to obtain a good statistical average.

The MD simulation for calculating the 2D-IR spectra was performed in a similar way, except that the number of molecules was limited to N = 32 and the time evolution period was shortened to about 32.6 ps, to carry out the calculations with the available computational resources. As a result, the frequency resolution of the calculated 2D-IR spectra is ∼2 cm^{-1}. Note that for half of this time evolution period (from t_1 to $t_1 + t_3$ in eqs 9 and 13), the vibrational Hamiltonian of the two-quantum excited states $H^{2Q}(\tau)$ [of dimension equal to $N(N+1)/2$] should be diagonalized. The 2D-IR spectra were smoothed with a Gaussian function with the fwhm of 8 cm^{-1}, and averaged over 1080 (for type I) or 540 (for type II) samples. To check the validity of the use of the N = 32 system, the polarized Raman spectrum and some other spectral quantities were also calculated for the N = 32 system and compared with the results for the N = 128 system.

The calculations were carried out on Hewlett-Packard zx6000 and other workstations with our original programs. Parts of the calculations were also carried out on TX-7 computers at the Research Center for Computational Science of the National Institutes of Natural Sciences at Okazaki. The computation time needed to calculate the 2D-IR spectra was equivalent to ∼2900 (for type I) and ∼6500 h (for type II) of a single zx6000 (Itanium-2, 1.5 GHz/6MB cache) CPU time. Since the calculations involve diagonalization of $H^{2Q}(\tau)$, whose dimension is equal to $N(N+1)/2$, the computational time is expected to scale as ∼$O(N^6)$ or ∼$O(N^7)$.

4. Results and Discussion

A. Noncoincidence Effect and Related Properties. The IR and Raman spectra in the amide I region calculated for liquid DMF (N = 128 system) are shown as solid lines in Figure 2a,b. The observed Raman spectrum taken from ref 18 is shown in Figure 2c for comparison. It is seen that the frequency positions of the IR, isotropic Raman, and anisotropic Raman bands are clearly separated from each other, meaning that there is a large magnitude of NCE. The calculated magnitude of the NCE

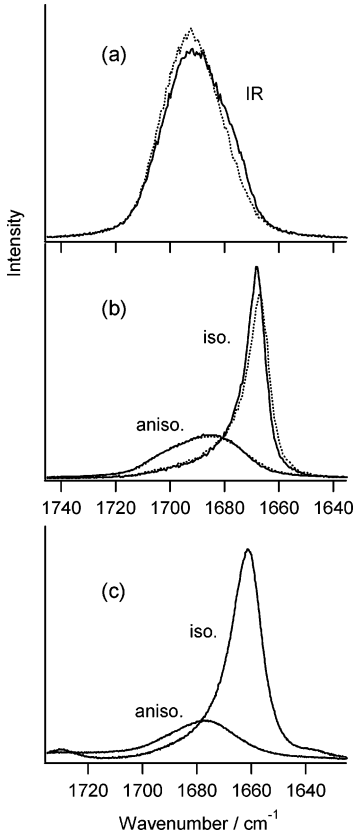

Figure 2. Calculated (a) IR and (b) polarized Raman spectra of the amide I band of liquid *N*,*N*-dimethylformamide (calculated with eqs 5 and 4, respectively): solid lines calculated for the $N = 128$ system and dotted lines calculated for the $N = 32$ system. (c) Observed polarized Raman spectrum taken from ref 18. The small peak at ~1636 cm^{-1} arises from the amide I mode of the naturally present ^{13}C-(carbonyl)-substituted species, and that at ~1730 cm^{-1} from the overtone state[77] of the mode consisting of the N−C(methyl) symmetric stretching combined with the OCN bending (of the normal species).

defined as $\omega_{NCE} \equiv \omega_{aniso} - \omega_{iso}$ (based on the first moments of these bands) is 14.7 cm^{-1}, in agreement with the observed value (14.6 cm^{-1}).[18] The calculated absolute frequency positions of the component bands ($\omega_{IR} = 1690.2$ cm^{-1}, $\omega_{iso} = 1673.3$ cm^{-1}, and $\omega_{aniso} = 1688.0$ cm^{-1}) are shifted from that of an isolated molecule by −24.8, −41.7, and −27.0 cm^{-1}, respectively. Considering that no electronic polarization effect is taken into account in the calculation,[9] these values are reasonable as compared with the observed values ($\Delta\omega_{iso} = -51$ cm^{-1} and $\Delta\omega_{aniso} = -36$ cm^{-1}).[18] It is also seen in Figure 2a,b that the calculated isotropic Raman band is significantly narrower than the calculated IR and the anisotropic Raman bands (Γ_{iso}(fwhm) = 8.3 cm^{-1} as compared with $\Gamma_{IR} = 29.3$ cm^{-1} and $\Gamma_{aniso} = 34.2$ cm^{-1}) and there is noticeable asymmetry in the band profile of the former. The calculation is in reasonable agreement with the experiment[18] ($\Gamma_{iso} \cong 14$ cm^{-1} and $\Gamma_{aniso} \cong 30$ cm^{-1}, see Figure 2c for the band asymmetry) also on these points. The difference in the bandwidth between the observed and calculated isotropic Raman spectra may be partly due to the neglect of the effect of vibrational population relaxation in the calculation. The results obtained for the $N = 32$ system are shown as dotted lines in Figure 2a,b. It is seen that the calculated spectral features are mainly the same as those obtained for the $N = 128$ system, suggesting the validity of the use of this size of system for the analysis of the 2D-IR spectral profiles described in section 4D.

Considering the agreement between the observed and calculated Raman spectral features obtained above as indicating the validity of the interaction mechanisms and the molecular parameters contained in the calculation, the time dependence of the transient IR absorption anisotropy is predicted by the calculation based on eqs 20−24. The result is shown in Figure 3. It is clearly seen that the transient IR absorption anisotropy decays very rapidly [from 0.4 to ~0.147 ($=0.4 \times e^{-1}$) in about 0.54 ps] in the case of neat liquid, where the off-diagonal vibrational couplings are fully operating, but the decay becomes much slower when all the off-diagonal vibrational couplings are switched off, e.g., in the case of an isotopically diluted solution (called "isolated case"). The latter is equivalent to the second-order time correlation function of the orientation of individual molecules (with regard to the directions of their transition dipoles). This result indicates that the rapid decay of the transient IR absorption anisotropy on the order of ~0.5 ps arises from the off-diagonal vibrational coupling.

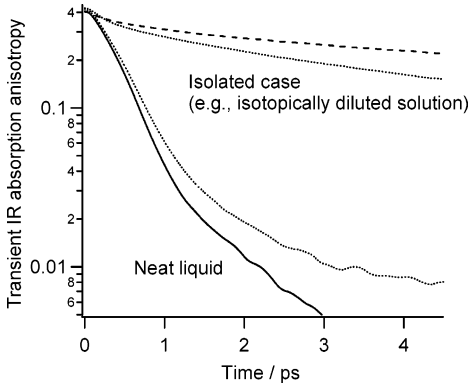

Figure 3. Time dependence of the transient IR absorption anisotropy calculated for the amide I mode of liquid *N*,*N*-dimethylformamide (calculated with eq 22): solid and broken lines are calculated for the neat liquid and isolated cases ($N = 128$), respectively, and dotted lines are the corresponding plots for the $N = 32$ system.

To see how this time constant is related to the rate of delocalization of vibrational modes, the time evolution of the extent of delocalization of the initially localized vibrational excitations [denoted as $d(t)$] is examined. It is expressed as[9]

$$d(t) = \left\langle \frac{1}{N}\sum_{m=1}^{N}\left(\sum_{n=1}^{N}|z_{nm}(t)|^4\right)^{-1} \right\rangle \qquad (25)$$

where $z_{nm}(t)$ is the transfer amplitude of the vibrational excitation from the mth to the nth molecule, defined as

$$z_{nm}(t) = \left\langle n \left| \exp_+\left[-\frac{i}{\hbar}\int_0^t d\tau\, H^{1Q}(\tau)\right] \right| m \right\rangle \qquad (26)$$

The result is shown in Figure 4. It is seen that initially localized vibrational excitations become delocalized over about 4 molecules in about 0.5 ps. In the case of the $N = 32$ system, $d(t)$ begins to saturate from about 1 ps with $N/2$ as the limiting value. For comparison, the results obtained[9] for the C═O stretching modes of neat liquid acetone and an acetone/dimethyl sulfoxide (DMSO) binary liquid mixture (mole fraction of acetone $x_{acetone} = 0.2$) are also shown in Figure 4. Considering that the magnitude of the NCE is decreasing in the order of DMF > acetone > acetone/DMSO ($x_{acetone} = 0.2$), and that the calculated Raman spectral profiles and the behavior of the transient IR absorption anisotropy are not significantly different between the $N = 128$ and 32 systems of DMF, it may be said that the initial delocalization speed of the vibrational excitations is intimately related to the features of the optical signals in the time and frequency domains. It is also suggested that the transient IR absorption

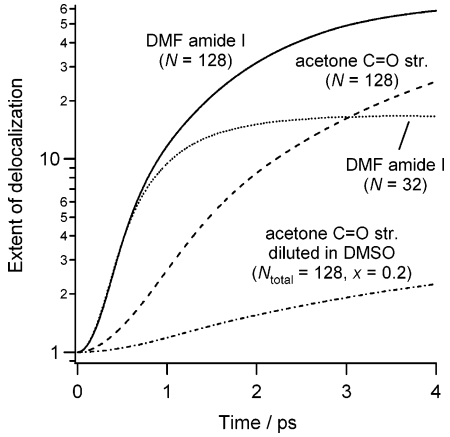

Figure 4. Time evolution of the extent of delocalization of the initially localized vibrational excitations $d(t)$ as defined by eq 25, calculated for the amide I mode of liquid *N*,*N*-dimethylformamide (solid and dotted lines for $N = 128$ and 32, respectively). The plots for the C═O stretching modes of liquid acetone ($N = 128$, broken line) and an acetone/dimethyl sulfoxide binary liquid mixture ($N_{total} = 128$ and $x_{acetone} = 0.2$, dot−dashed line) taken from ref 9 are also shown.

anisotropy decays in the time needed for the initially localized vibrational excitations to delocalize over a few molecules.

B. Spectra in the Static Case and Participation Ratio. As a reference to the above calculation, to see the effect of liquid dynamics on the band profiles, the spectra in the static case are also calculated by freezing all the liquid dynamics. The result is shown in Figure 5. Compared with the spectra in Figure 2, it is seen that the effect of liquid dynamics is most noticeable in the profile of the isotropic Raman band. In a similar way to the case of the C═O stretching band of liquid acetone shown in our previous study,[9] there is a small bump at ∼1710 cm^{-1} on this band in the static case as shown in Figure 5b, but it disappears from the effect of liquid dynamics as shown in Figure 2b. In addition, the peak frequency position is slightly shifted (from 1664 cm^{-1} in Figure 5b to 1668 cm^{-1} in Figure 2b) and the band is narrowed (from $\Gamma_{iso} = 10.3$ cm^{-1} in Figure 5b to 8.3 cm^{-1} in Figure 2b) by the effect of liquid dynamics. These changes are reasonably explained by the motional narrowing effect. A similar narrowing effect is also seen in the IR (from $\Gamma_{IR} = 35.2$ to 29.3 cm^{-1}) and anisotropic Raman (from $\Gamma_{aniso} = 38.9$ to 34.2 cm^{-1}) bands. As described below in section 4C, the time scale of the frequency modulation is about 0.14 ps and in the so-called fast modulation regime.

The spectrum in the isolated (and static) case is shown in Figure 5d. Taking the width of this band (19.4 cm^{-1}) as a reference, the isotropic Raman band is narrowed and the IR and anisotropic Raman bands are broadened by the effect of the resonant off-diagonal vibrational coupling. Note that there is no NCE in the isolated case, so that the band profiles of the IR, isotropic Raman, and anisotropic Raman spectra are the same when we (additionally) freeze the liquid dynamics.

The extent of delocalization of vibrational modes in the static case is evaluated by calculating the frequency-dependent participation ratio $\eta(\omega)$ defined as[67−70]

$$\eta(\omega) = \frac{\left\langle \sum_{\xi=1}^{N} \left(\sum_{m=1}^{N} c_{m\xi}^{4} \right)^{-1} \delta(\omega - \omega_{\xi}) \right\rangle}{\left\langle \sum_{\xi=1}^{N} \delta(\omega - \omega_{\xi}) \right\rangle} \tag{27}$$

where $c_{m\xi}$ is the normalized vibrational amplitude of the mth molecule in the ξth mode, and ω_{ξ} is the vibrational frequency of the ξth mode. The result is shown in Figure 5e. It is seen that the vibrational modes around the band center are delocalized over ∼30 molecules in the case of the $N = 128$ system, but over ∼10 molecules in the case of the $N = 32$ system. Considering the behavior of $d(t)$ shown in Figure 4, as well as the fact that the frequency-domain picture corresponds to the long-time behavior of the system, the dependence of the value of $\eta(\omega)$ on the system size is related to the saturation of $d(t)$ after 1 ps for the $N = 32$ system. As discussed in the last part of section 4A, the features of optical signals in the time and frequency domains induced by resonant off-diagonal vibrational coupling are considered to be related to the initial delocalization speed of the vibrational excitations. This means that the participation ratio may not be a good measure of the extent of delocalization of vibrational modes with regard to the relation with those features of optical signals in the presence of fast frequency modulations.

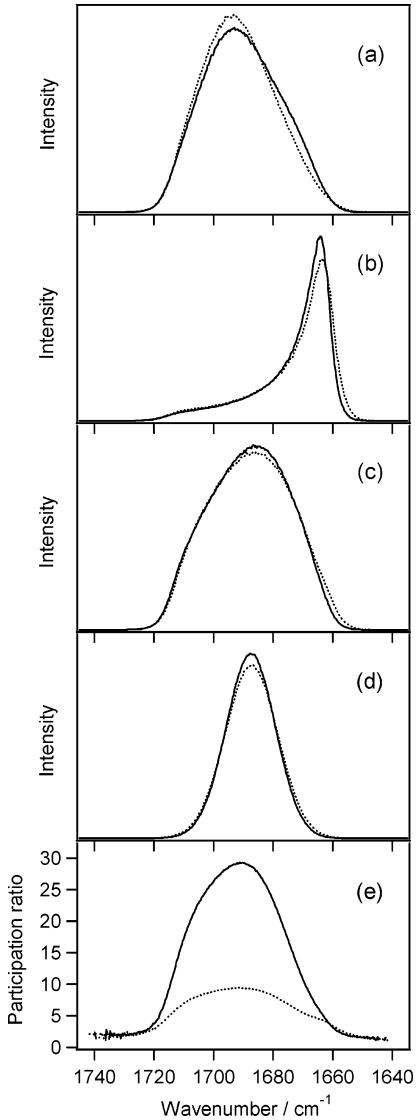

Figure 5. (a) IR, (b) isotropic Raman, and (c) anisotropic Raman spectra of the amide I band of liquid *N*,*N*-dimethylformamide calculated in the static case, (d) the spectrum in the isolated and static case, and (e) the frequency-dependent participation ratio $\eta(\omega)$ as defined by eq 27: solid lines are calculated for the $N = 128$ system and dotted lines are calculated for the $N = 32$ system.

C. Modulations of Various Quantities. To see the nature of the modulations induced by the liquid dynamics in more

detail, time correlation functions are calculated for various quantities. The time correlation function $C_L(t)$ of the modulations of the vibrational frequencies of individual molecules is defined as

$$C_L(t) = \left\langle \frac{1}{N}\sum_{m=1}^{N} \delta\omega_m^{(L)}(t)\delta\omega_m^{(L)}(0) \right\rangle \tag{28}$$

where

$$\delta\omega_m^{(L)}(t) = \omega_m^{(L)}(t) - \left\langle \frac{1}{N}\sum_{m=1}^{N} \omega_m^{(L)} \right\rangle \tag{29}$$

and $\omega_m^{(L)}(t)$ is the (uncoupled) vibrational frequency of the mth molecule [equal to the mth diagonal element of the vibrational Hamiltonian, $H_{mm}^{1Q}(t)$] at time t. The result is shown in Figure 6a. It is seen that the time dependence of $C_L(t)/C_L(0)$ around $t \cong 0$ is approximated as $1 - (u_2/2)t^2 + O(t^4)$ with $u_2 > 0$. Employing the stationary nature of the frequency modulations,[82] we have

$$u_2 = \left\langle \frac{1}{N}\sum_{m=1}^{N} \left(\frac{d}{dt}\delta\omega_m^{(L)}(t) \right)^2 \Big|_{t=0} \right\rangle \Big/ \left\langle \frac{1}{N}\sum_{m=1}^{N} (\delta\omega_m^{(L)}(0))^2 \right\rangle \tag{30}$$

meaning that the time scale of the frequency modulation is obtained from the value of u_2. From the fitting to the plot of $C_L(t)/C_L(0)$ in the $t = 0.00-0.08$ ps range, we have $u_2 = 50.1$ ps^{-2}. Taking the inverse of the square root of u_2,[83] we obtain $\tau_f = 0.14$ ps as the time scale of the modulation of $\omega_m^{(L)}(t)$. Combining with the value of Δ_f ($\equiv\sqrt{C_L(0)}$) $= 8.3$ cm^{-1}, we have $2\pi c\tau_f\Delta_f = 0.22$, which is significantly smaller than unity, meaning that the frequency modulation occurs in the fast modulation regime.[84]

By contrast, the time correlation function $C_N(t)$ of the vibrational frequencies $\omega_\xi(t)$ of the eigenstates of $H^{1Q}(t)$ defined as

$$C_N(t) = \left\langle \frac{1}{N}\sum_{\xi=1}^{N} \delta\omega_\xi(t)\delta\omega_\xi(0) \right\rangle \tag{31}$$

with

$$\delta\omega_\xi(t) = \omega_\xi(t) - \left\langle \frac{1}{N}\sum_{\xi=1}^{N} \omega_\xi \right\rangle \tag{32}$$

is almost invariant and is essentially equal to unity (not shown) if we number the eigenstates in the sequence of their vibrational frequencies. Instead, the nature of individual eigenstates changes as time evolves because of the avoided crossings among them. To see this in a quantitative way, we have calculated the following time correlation functions. The time correlation function $C_{IR}(t)$ of the IR intensities is defined as

$$C_{IR}(t) = \left\langle \frac{1}{N}\sum_{\xi=1}^{N} \delta S_\xi^{(IR)}(t)\delta S_\xi^{(IR)}(0) \right\rangle \tag{33}$$

where

$$\delta S_\xi^{(IR)}(t) = S_\xi^{(IR)}(t) - \left\langle \frac{1}{N}\sum_{\xi=1}^{N} S_\xi^{(IR)} \right\rangle \tag{34}$$

is the instantaneous difference in the IR intensity $S_\xi^{(IR)}(t)$ of the ξth eigenstate from the average value. The time correlation functions of the isotropic and anisotropic Raman intensities, $C_{iso}(t)$ and $C_{aniso}(t)$, are defined in a similar way. The changes in the nature of the eigenstates are also seen in the correlation function of the "mode identity" $M(t)$, expressed as[73]

$$M(t) = \left\langle \frac{1}{N}\sum_{\xi=1}^{N} \max_{1\le\zeta\le N}\{|\langle\zeta_t|\xi_0\rangle|^2\} \right\rangle \tag{35}$$

The results are shown in Figure 6b−e. It is seen that all these quantities are modulated in subpicosecond time scales. This is the picture of the effect of liquid dynamics on the vibrational properties obtained on the eigenstate basis, which corresponds to the picture obtained on the molecular basis shown in Figure

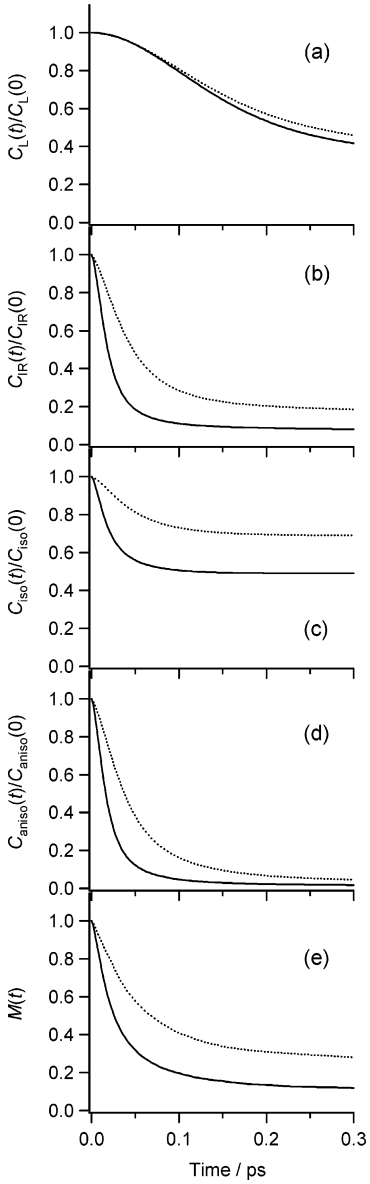

Figure 6. (a) Normalized time correlation function of the modulations of the vibrational frequencies of individual molecules, $C_L(t)/C_L(0)$ defined by eq 28, (b) normalized time correlation function of the modulations of the IR intensities of the eigenstates, $C_{IR}(t)/C_{IR}(0)$ defined by eq 33, (c, d) the same type of time correlation functions calculated for the isotropic and anisotropic Raman intensities, and (e) time correlation function of the "mode identity" $M(t)$ defined by eq 35, calculated for the amide I mode of liquid *N*,*N*-dimethylformamide: solid lines are calculated for the $N = 128$ system and dotted lines are calculated for the $N = 32$ system.

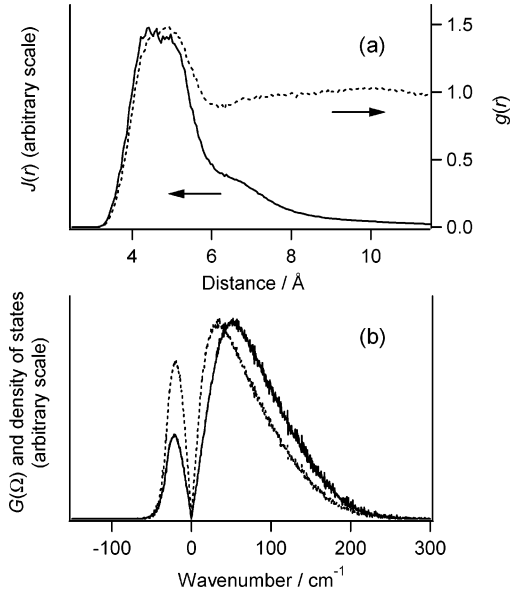

Figure 7. (a) Solid line: spatial distribution of the molecules that modulate the electric field effective on the frequency of the amide I mode, $J(r)$ (average of $J_m(r)$ defined by eq 36 over $m = 1-N$). Broken line: radial distribution function $g(r)$, calculated for liquid *N*,*N*-dimethylformamide ($N = 128$). (b) Solid line: frequency distribution of the motions (concerning the liquid dynamics, i.e., intermolecular degrees of freedom) that modulate the electric field effective on the frequency of the amide I mode, $G(\Omega)$ (average of $G_m(\Omega)$ defined by eq 37 over $m = 1 - N$). Broken line: density of states of the instantaneous normal modes.

6a. In other words, the modulations appear in the vibrational frequencies in the picture on the molecular basis and in the vibrational transition intensities and the nature of the modes in the picture on the eigenstate basis. It is also true, however, that the behavior of the correlation functions in Figure 6b−e is somewhat dependent on the system size, meaning that they should be interpreted carefully.

Considering that the vibrational frequencies of individual molecules are supposed to be controlled by the electric field from the surrounding molecules as shown in eq 14, the nature of the liquid dynamics that modulates the vibrational properties is examined in some detail with the concept of the field-modulating modes (FMMs).[7] Within this picture, the spatial distribution of the molecules that modulate the electric field on the *m*th molecule (effective in the frequency modulation of its amide I mode) is expressed as

$$J_m(r) = \left\langle \sum_{n=1}^{N} \sum_{j=1}^{6} \left(\frac{\partial E_{\parallel,m}}{\partial R_{j,n}} \right)^2 \delta(r - r_{nm}) \right\rangle \qquad (36)$$

where $E_{\parallel,m}$ is the electric field on the *m*th molecule in the direction parallel to the dipole derivative of its amide I mode, and $R_{j,n}$ stands for the normalized translational ($j = 1-3$) and rotational ($j = 4-6$) coordinates of the *n*th molecule. The center of the C═O bond, which is the interaction point in constructing the vibrational Hamiltonian as described in section 3, is taken as the location where $E_{\parallel,m}$ is evaluated, and also as the reference point in the *m*th molecule for calculating r_{nm}. The result (the average of $J_m(r)$ over $m = 1 - N$, denoted as $J(r)$) is shown in Figure 7a (solid line). Compared with the radial distribution function $g(r)$ (dotted line), it is recognized that the electric field operating on a specified molecule (the *m*th molecule in eq 36) is modulated mainly by the motions of the molecules in the first solvation shell (within ∼6 Å) and additionally by those

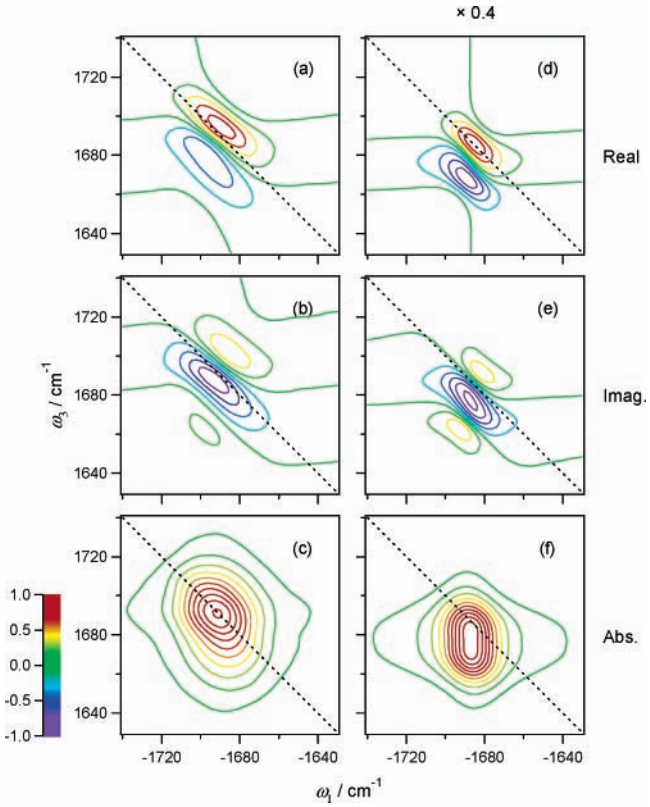

Figure 8. (a−c) The real and imaginary parts and the absolute value 2D-IR spectra of the type I optical processes with the *zzzz* polarization calculated for the amide I band of liquid *N*,*N*-dimethylformamide and (d−f) the corresponding spectra in the isolated case. The latter spectra are multiplied by the factor of 0.4 (i.e., the peak intensities in the latter spectra are actually higher by the factor of ∼2.5 than those in the former). The color code for the relative intensities is indicated on the lower left corner.

within ∼8 Å. It is also possible to evaluate the frequency distribution of those field-modulating motions in the same FMM picture, by calculating the function $G_m(\Omega)$ defined as[7]

$$G_m(\Omega) = \left\langle \sum_{s=1}^{6N} \left(\frac{\partial E_{\parallel,m}}{\partial Q_s} \right)^2 \delta(\Omega - \Omega_s) \right\rangle \qquad (37)$$

where Q_s is the *s*th instantaneous normal mode of the intermolecular degrees of freedom (consisting of translations and rotations, $\{R_{j,n}\}_{1\le j\le 6, 1\le n\le N}$), and Ω_s is its vibrational frequency. The result (the average of $G_m(\Omega)$ over $m = 1 - N$, denoted as $G(\Omega)$) is shown in Figure 7b (solid line).[85] Compared with the density of states (dotted line), it is seen that the intermolecular vibrational motions in the 50−200 cm^{-1} region are likely to modulate the electric field to a greater extent than those in the lower frequency region.

D. 2D-IR Spectra. The calculated 2D-IR spectrum of the type I processes with the *zzzz* polarization is shown in Figure 8a−c. The two frequency axes ω_1 and ω_3 correspond to the time intervals t_1 and t_3, respectively. The two peaks (in the opposite signs) along the ω_3 axis in the real part of the spectrum correspond to the $v = 0 \rightarrow 1$ and $1 \rightarrow 2$ transition frequencies. The bands are elongated along the diagonal of the spectrum because of the distribution of the transition frequencies.

To see the effect of the resonant off-diagonal vibrational coupling and the delocalization of vibrational modes in the 2D-IR spectral profiles, the spectrum in the "isolated case", where all the off-diagonal vibrational couplings in $H^{1Q}(\tau)$ and $H^{2Q}(\tau)$ are switched off, is also calculated and shown in Figure 8d−f.

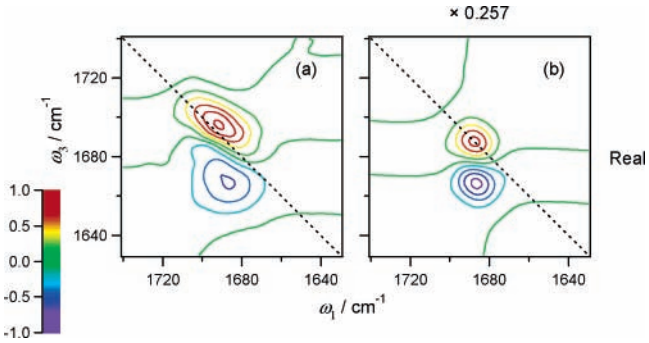

Figure 9. (a) The real-part 2D-IR "absorptive" spectrum with the *zzzz* polarization calculated for the amide I band of liquid *N*,*N*-dimethylformamide and (b) the corresponding spectrum in the isolated case. The latter spectrum is multiplied by the factor of 0.257. The color code for the relative intensities is indicated on the lower left corner.

The most notable difference is that, in the real part of the spectrum, the peak of the positive band is located on the diagonal *with the same intensity as the negative band* in the isolated case (Figure 8d), while it is shifted off the diagonal to the upper triangle *with an asymmetric intensity pattern* when the vibrational coupling is operating (Figure 8a). The difference is also seen in the imaginary part of the spectrum as the asymmetry in the intensities of the positive bands in the spectrum (Figure 8b vs 8e). These differences in the intensity patterns of the real and imaginary parts are also reflected in those of the absolute value spectra (Figure 8c,f). In the isolated case, the plateau corresponding to the peaks of the real and imaginary parts is seen (Figure 8f), while a single peak is seen when the vibrational coupling is operating (Figure 8c).

These differences in the band profile are considered to arise from the specific situation realized in the presence of the resonant off-diagonal vibrational coupling. As shown in eqs 16 and 18, although there is strong vibrational coupling among the one-quantum excited states as well as among the combination states, there is no direct coupling among the overtone states. In other words, there is little frequency dispersion induced by the resonant off-diagonal vibrational coupling for the overtone states. As a result, the transition frequencies in the t_1 and t_3 time intervals in the R_3 diagram are anti-correlated when an overtone state is involved. Adding the broadening due to the distribution of the diagonal terms, we obtain the real-part spectrum with the negative band being broadened along the anti-diagonal to a greater extent than the positive band, as shown in Figure 8a. It is possible to explain in the same way the band profile of the imaginary-part spectrum shown in Figure 8b.

The calculated "absorptive" 2D-IR spectrum (the sum of the spectra of the type I and type II processes) with the *zzzz* polarization is shown in Figure 9a. The corresponding spectrum in the isolated case is shown in Figure 9b. Considering that the absorptive spectrum is obtained for the purpose of removing the dispersive part of the spectrum, only the real-part spectrum is shown. It is seen that the asymmetry in the intensity pattern as seen in Figure 8a is also recognized in Figure 9a when the vibrational coupling is operating. In addition, weak elongation along the diagonal is also present. In contrast, in the isolated case, there is no elongation of the bands along the diagonal because of the cancellation of the elongation effect between the spectra of the type I and type II processes (Figure 9b). A detailed comparison of the spectral profiles between the type I and type II processes and with the spectrum of another set of optical processes (called type III) will be shown elsewhere.

It has been discussed that the effect of the off-diagonal vibrational coupling is more clearly seen by eliminating the

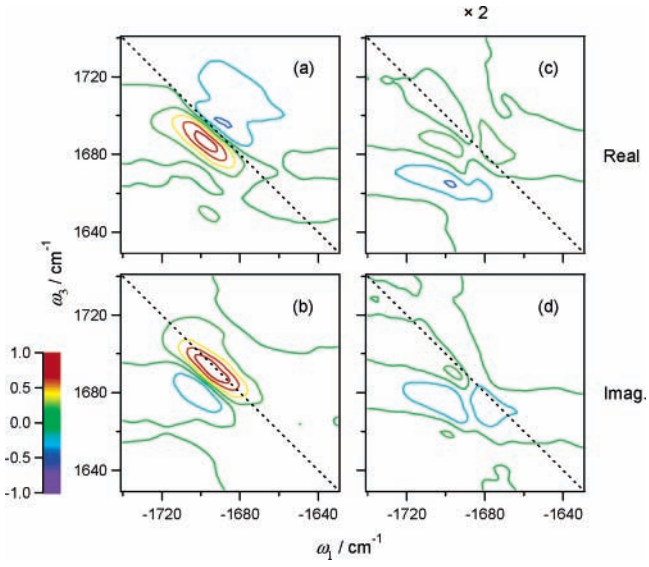

Figure 10. (a, b) The real and imaginary parts of the difference between the 2D-IR spectra of the type I processes with the *zzzz* and *zxxz* polarizations, calculated as $S_{zzzz} - 3S_{zxxz}$, for the amide I band of liquid *N*,*N*-dimethylformamide and (c, d) the corresponding spectra in the isolated case. The former spectra are magnified by the factor of 3.4 as compared with the spectra in Figure 8a−c, and the latter spectra are further magnified by the factor of 2. The color code for the relative intensities is indicated on the lower left corner.

diagonal peaks in the 2D-IR spectra with the use of specific polarization conditions.[36,60,61] One way is to take the difference between the spectra with the *zzzz* and *zxxz* polarizations as $S_{zzzz} - 3S_{zxxz}$.[36,60] The 2D-IR spectrum calculated this way for the type I processes is shown in Figure 10a,b. The corresponding spectrum in the isolated case is shown in Figure 10c,d. It is seen that some bands of significant intensities are present when the vibrational coupling is operating, but the signals are much weaker when the vibrational coupling is switched off. Considering that the spectral intensities in Figure 10c,d are magnified by the factor of 17 (=3.4 × 2/0.4) as compared with those in Figure 8d−f, we may regard that essentially all the spectral features in Figure 8d−f are canceled by taking the difference as $S_{zzzz} - 3S_{zxxz}$.

Since all the spectral features are "diagonal" in the isolated case, it is reasonable that they are canceled by taking the difference as $S_{zzzz} - 3S_{zxxz}$. In contrast, the existence of some bands in the presence of the off-diagonal vibrational coupling is considered to be closely related to the rapid depolarization of the IR excitations shown in Figure 3. Because the anisotropy of the IR excitations becomes rapidly reduced on the order of ~1 ps, the relative intensity of S_{zxxz} (as compared with that of S_{zzzz}) is enhanced to some extent, giving rise to the spectral features of $S_{zzzz} - 3S_{zxxz}$ that look like a kind of "over-cancellation" of the features of S_{zzzz}. This result indicates that we can clearly see the effect of the off-diagonal vibrational coupling by observing the spectra of $S_{zzzz} - 3S_{zxxz}$.

Another method that has been suggested for eliminating the diagonal peaks in the 2D-IR spectra is to set the polarization as S_{xzqp} with $p = (x + z)/\sqrt{2}$ and $q = (x - z)/\sqrt{2}$.[61] The spectrum calculated for the type I processes with this polarization and the corresponding spectrum in the isolated case are shown in Figure 11, parts a,b and c,d, respectively. It is seen that, in this case also, some bands of significant intensities are present when the vibrational coupling is operating, but the band intensities are weaker when the vibrational coupling is switched off. However, the contrast in the band intensities is more clearly

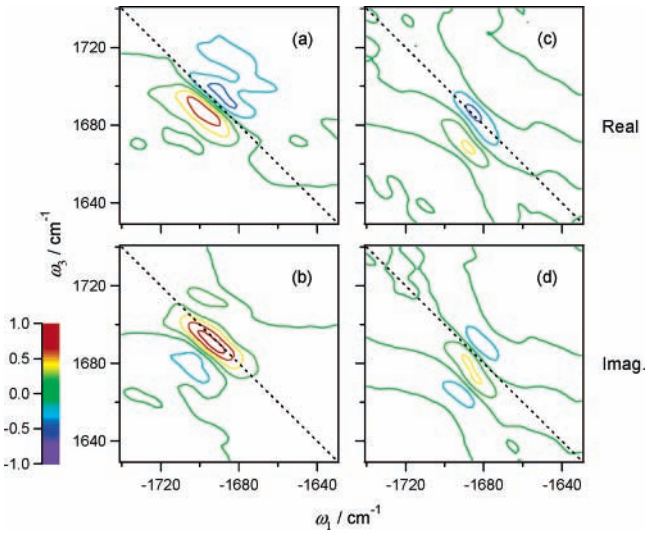

Figure 11. (a, b) The real and imaginary parts of the 2D-IR spectra of the type I processes, calculated by setting the polarization condition as *xzqp* with $p = (x + z)/\sqrt{2}$ and $q = (x - z)/\sqrt{2}$, for the amide I band of liquid *N*,*N*-dimethylformamide, and (c, d) the corresponding spectra in the isolated case. The color code for the relative intensities is indicated on the lower left corner.

noticeable in Figure 10 than in Figure 11, suggesting that the spectrum of $S_{zzzz} - 3S_{zxxz}$ is more appropriate for observing the effect of the off-diagonal vibrational coupling.

5. Summary

In the present paper, a time-domain method for calculating polarized Raman and 2D-IR spectra that includes the effects of both the diagonal frequency modulations and the off-diagonal vibrational coupling is presented, and is applied to the case of the amide I band of liquid DMF. On the basis of the agreement between the observed and calculated band profiles of the polarized Raman spectrum, the time dependence of the transient IR absorption anisotropy is also predicted.

The main conclusions obtained in this study may be summarized as follows. (1) The effect of the resonant off-diagonal vibrational coupling and the resulting delocalization of vibrational modes is clearly seen as the NCE in the polarized Raman spectrum, the rapid decay of the transient IR absorption anisotropy, and some spectral features (especially as asymmetric intensity patterns) in the 2D-IR spectra. Concerning the selection of the polarization condition of the 2D-IR spectra, taking the difference as $S_{zzzz} - 3S_{zxxz}$ is suggested to be most appropriate for observing this effect. (2) The features of the optical signals in the time and frequency domains arising from the effect of resonant off-diagonal vibrational coupling described above are considered to be related to the initial delocalization speed of the vibrational excitations evaluated as $d(t)$ defined by eq 25. The participation ratio $\eta(\omega)$ defined by eq 27 seems to be less relevant in the presence of fast frequency modulations. (3) From the value of $2\pi c\tau_f\Delta_f = 0.22$, which is significantly smaller than unity, the diagonal frequency modulations are considered to be in the fast modulation regime. As a result, some differences in the spectral profiles are seen between the cases where the liquid dynamics is active (Figure 2) and where it is frozen (Figure 5). In the picture on the eigenstate basis, the modulations appear in the vibrational transition intensities (Figure 6b−e) instead of vibrational frequencies. The motions (concerning the liquid dynamics) of the molecules in the first solvation shell (within ~6 Å) and in the 50−200 cm^{-1} region are likely to participate mainly in those modulations.

The results in the present study clearly demonstrate that the spectral features obtained with the polarized Raman, transient IR, and 2D-IR spectroscopic methods may be analyzed with both the diagonal frequency modulations and the off-diagonal vibrational coupling taken into account in the presence of fast liquid dynamics. It is expected that this theoretical method helps to elucidate the nature of the dynamics and intermolecular interactions and the behavior of the vibrational excitations in relation to the spectral features for various liquid-phase systems and other related systems such as polypeptides and proteins.

Acknowledgment. This study was supported by a Grant-in-Aid for Scientific Research from the Ministry of Education, Culture, Sports, Science, and Technology. The author would like to thank Maria Grazia Giorgini and Maurizio Musso for providing the observed polarized Raman spectrum of ref 18.

References and Notes

(1) Torii, H. In *Novel Approaches to the Structure and Dynamics of Liquids*: *Experiments, Theories and Simulations*; Samios, J., Durov. V. A., Eds.; Kluwer: Dordrecht, The Netherlands, 2004; p 343.
(2) Ham, S.; Kim, J. H.; Lee, H.; Cho, M. *J. Chem. Phys.* **2003**, *118*, 3491.
(3) Bouř, P.; Keiderling, T. A. *J. Chem. Phys.* **2003**, *119*, 11253.
(4) Fecko, C. J.; Eaves, J. D.; Loparo, J. J.; Tokmakoff, A.; Geissler, P. L. *Science* **2003**, *301*, 1698.
(5) Corcelli, S. A.; Lawrence, C. P.; Skinner, J. L. *J. Chem. Phys.* **2004**, *120*, 8107.
(6) Schmidt, J. R.; Corcelli, S. A.; Skinner, J. L. *J. Chem. Phys.* **2004**, *121*, 8887.
(7) Torii, H. *J. Phys. Chem. A* **2002**, *106*, 1167.
(8) Torii, H. *J. Phys. Chem. A* **2004**, *108*, 7272.
(9) Torii, H.; Musso, M.; Giorgini, M. G. *J. Phys. Chem. A* **2005**, *109*, 7797.
(10) Fini, G.; Mirone, P.; Fortunato, B. *J. Chem. Soc., Faraday Trans. 2* **1973**, *69*, 1243.
(11) Perchard, C.; Perchard, J. P. *J. Raman Spectrosc.* **1975**, *3*, 277.
(12) Schindler, W.; Sharko, P. T.; Jonas, J. *J. Chem. Phys.* **1982**, *76*, 3493.
(13) Zerda, T. W.; Thomas, H. D.; Bradley, M.; Jonas, J. *J. Chem. Phys.* **1987**, *86*, 3219.
(14) Sokolowska, A.; Kecki, Z. *J. Raman Spectrosc.* **1993**, *24*, 331.
(15) Mortensen, A.; Faurskov Nielsen, O.; Yarwood, J.; Shelley, V. *J. Phys. Chem.* **1994**, *98*, 5221.
(16) Bertie, J. E.; Michaelian, K. H. *J. Chem. Phys.* **1998**, *109*, 6764.
(17) Schweitzer-Stenner, R.; Sieler, G.; Mirkin, N. G.; Krimm, S. *J. Phys. Chem. A* **1998**, *102*, 118.
(18) Giorgini, M. G.; Musso, M.; Asenbaum, A.; Döge, G. *Mol. Phys.* **2000**, *98*, 783.
(19) McHale, J. L. *J. Chem. Phys.* **1981**, *75*, 30.
(20) Logan, D. E. *Chem. Phys.* **1986**, *103*, 215.
(21) Torii, H.; Tasumi, M. *J. Chem. Phys.* **1993**, *99*, 8459.
(22) Musso, M.; Giorgini, M. G.; Döge, G.; Asenbaum, A. *Mol. Phys.* **1997**, *92*, 97.
(23) Giorgini, M. G.; Fini, G.; Mirone, P. *J. Chem. Phys.* **1983**, *79*, 639.
(24) Kamoun, M.; Mirone, P. *Chem. Phys. Lett.* **1980**, *75*, 287.
(25) Musso, M.; Torii, H.; Ottaviani, P.; Asenbaum, A.; Giorgini, M. G. *J. Phys. Chem. A* **2002**, *106*, 10152.
(26) Giorgini, M. G.; Musso, M.; Torii, H. *J. Phys. Chem. A* **2005**, *109*, 5846.
(27) Musso, M.; Giorgini, M. G.; Torii, H.; Dorka, R.; Schiel, D.; Asenbaum, A.; Keutel, D.; Oehme, K.-L. *J. Mol. Liq.* In press.
(28) Miyazawa, T.; Blout, E. R. *J. Am. Chem. Soc.* **1961**, *83*, 712.
(29) Krimm, S.; Abe, Y. *Proc. Natl. Acad. Sci. U.S.A.* **1972**, *69*, 2788.
(30) Byler, D. M.; Susi, H. *Biopolymers* **1986**, *25*, 469.
(31) Torii, H.; Tasumi, M. *J. Chem. Phys.* **1992**, *96*, 3379.
(32) Torii, H.; Tasumi, M. *J. Raman Spectrosc.* **1998**, *29*, 81.
(33) Surewitz, W. K.; Mantsch, H. H.; Chapman, D. *Biochemistry* **1993**, *32*, 389.
(34) Hamm, P.; Lim, M.; Degrado, W. F.; Hochstrasser, R. M. *Proc. Natl. Acad. Sci. U.S.A.* **1999**, *96*, 2036.
(35) Moran, A. M.; Park, S.-M.; Mukamel, S. *J. Chem. Phys.* **2003**, *118*, 9971.
(36) Woutersen, S.; Hamm, P. *J. Phys. Chem. B* **2000**, *104*, 11316.
(37) Schweitzer-Stenner, R.; Eker, F.; Huang, Q.; Griebenow, K. *J. Am. Chem. Soc.* **2001**, *123*, 9628.

(38) Eker, F.; Griebenow, K.; Cao, X.; Nafie, L. A.; Schweitzer-Stenner, R. *Biochemistry* **2004**, *43*, 613.
(39) Watson, T. M.; Hirst, J. D. *J. Phys. Chem. A* **2003**, *107*, 6843.
(40) Huang, R.; Kubelka, J.; Barber-Armstrong, W.; Silva, R. A. G. D.; Decatur, S. M.; Keiderling, T. A. *J. Am. Chem. Soc.* **2004**, *126*, 2346.
(41) Bouř, P.; Keiderling, T. A. *J. Phys. Chem. B* **2005**, *109*, 5348.
(42) Mikhonin, A. V.; Asher, S. A. *J. Phys. Chem. B* **2005**, *109*, 3047.
(43) Piryatinski, A.; Tretiak, S.; Chernyak, V.; Mukamel, S. *J. Raman Spectrosc.* **2000**, *31*, 125.
(44) Cha, S.; Ham, S.; Cho, M. *J. Chem. Phys.* **2002**, *117*, 740.
(45) Ham, S.; Cha, S.; Choi, J.-H.; Cho, M. *J. Chem. Phys.* **2003**, *119*, 1451.
(46) Mu, Y.; Kosov, D. S.; Stock, G. *J. Phys. Chem. B* **2003**, *107*, 5064.
(47) Woutersen, S.; Bakker, H. J. *Nature* **1999**, *402*, 507.
(48) Cowan, M. L.; Bruner, B. D.; Huse, N.; Dwyer, J. R.; Chugh, B.; Nibbering, E. T. J.; Elsaesser, T.; Miller, R. J. D. *Nature* **2005**, *434*, 199.
(49) Torii, H. *Chem. Phys. Lett.* **2000**, *323*, 382.
(50) Asplund, M. C.; Lim, M.; Hochstrasser, R. M. *Chem. Phys. Lett.* **2000**, *323*, 269.
(51) Zhao, W.; Wright, J. C. *Phys. Rev. Lett.* **2000**, *84*, 1411.
(52) Woutersen, S.; Mu, Y.; Stock, G.; Hamm, P. *Chem. Phys.* **2001**, *266*, 137.
(53) Mukherjee, P.; Krummel, A. T.; Fulmer, E. C.; Kass, I.; Arkin, I. T.; Zanni, M. T. *J. Chem. Phys.* **2004**, *120*, 10215.
(54) Ge, N.-H.; Hochstrasser, R. M. *PhysChemComm* **2002**, *5*, 17.
(55) Chung, H. S.; Khalil, M.; Tokmakoff, A. *J. Phys. Chem. B* **2004**, *108*, 15332.
(56) Wang, J.; Hochstrasser, R. M. *Chem. Phys.* **2004**, *297*, 195.
(57) Cheatum, C. M.; Tokmakoff, A.; Knoester, J. *J. Chem. Phys.* **2004**, *120*, 8201.
(58) Ham, S.; Hahn, S.; Lee, C.; Kim, T.-K.; Kwak, K.; Cho, M. *J. Phys. Chem. B* **2004**, *108*, 9333.
(59) Dijkstra, A. G.; Knoester, J. *J. Phys. Chem. B* **2005**, *109*, 9787.
(60) Zanni, M. T.; Gnanakaran, S.; Stenger, J.; Hochstrasser, R. M. *J. Phys. Chem. B* **2001**, *105*, 6520.
(61) Zanni, M. T.; Ge, N.-H.; Kim, Y. S.; Hochstrasser, R. M. *Proc. Natl. Acad. Sci. U.S.A.* **2001**, *98*, 11265.
(62) Fulmer, E. C.; Mukherjee, P.; Krummel, A. T.; Zanni, M. T. *J. Chem. Phys.* **2004**, *120*, 8067.
(63) Demirdöven, N.; Cheatum, C. M.; Chung, H. S.; Khalil, M.; Knoester, J.; Tokmakoff, A. *J. Am. Chem. Soc.* **2004**, *126*, 7981.
(64) Piryatinski, A.; Chernyak, V.; Mukamel, S. *Chem. Phys.* **2001**, *266*, 311.
(65) Kwac, K.; Cho, M. *J. Chem. Phys.* **2003**, *119*, 2256.
(66) Kato, T.; Tanimura, Y. *J. Chem. Phys.* **2004**, *120*, 260.
(67) Bell, R. J.; Dean, P. *Discuss. Faraday Soc.* **1970**, *50*, 55.
(68) Thouless, D. J. *Phys. Rep.* **1974**, *13*, 93.
(69) Weaire, D.; Williams, A. R. *J. Phys. C: Solid State Phys.* **1977**, *10*, 1239.
(70) Evensky, D. A.; Scalettar, R. T.; Wolynes, P. G. *J. Phys. Chem.* **1990**, *94*, 1149.
(71) A brief communication on this subject has been published: Torii, H. *Chem. Phys. Lett.* **2005**, *414*, 417.
(72) Mukamel, S. *Principles of Nonlinear Optical Spectroscopy*; Oxford University Press: New York, 1995.
(73) Torii, H. *J. Phys. Chem. A* **2002**, *106*, 3281.
(74) Hush, N. S.; Reimers, J. R. *J. Phys. Chem.* **1995**, *99*, 15798.
(75) Andrews, S. S.; Boxer, S. G. *J. Phys. Chem. A* **2002**, *106*, 469.
(76) Torii, H. *J. Chem. Phys.* **2003**, *119*, 2192.
(77) Jao, T. C.; Scott, I.; Steele, D. *J. Mol. Spectrosc.* **1982**, *92*, 1.
(78) Steele, D.; Quatermain, A. *Spectrochim. Acta* **1987**, *43A*, 781.
(79) Frisch, M. J.; Trucks, G. W.; Schlegel, H. B.; Scuseria, G. E.; Robb, M. A.; Cheeseman, J. R.; Montgomery, J. A., Jr.; Vreven, T.; Kudin, K. N.; Burant, J. C.; Millam, J. M.; Iyengar, S. S.; Tomasi, J.; Barone, V.; Mennucci, B.; Cossi, M.; Scalmani, G.; Rega, N.; Petersson, G. A.; Nakatsuji, H.; Hada, M.; Ehara, M.; Toyota, K.; Fukuda, R.; Hasegawa, J.; Ishida, M.; Nakajima, T.; Honda, Y.; Kitao, O.; Nakai, H.; Klene, M.; Li, X.; Knox, J. E.; Hratchian, H. P.; Cross, J. B.; Bakken, V.; Adamo, C.; Jaramillo, J.; Gomperts, R.; Stratmann, R. E.; Yazyev, O.; Austin, A. J.; Cammi, R.; Pomelli, C.; Ochterski, J. W.; Ayala, P. Y.; Morokuma, K.; Voth, G. A.; Salvador, P.; Dannenberg, J. J.; Zakrzewski, V. G.; Dapprich, S.; Daniels, A. D.; Strain, M. C.; Farkas, O.; Malick, D. K.; Rabuck, A. D.; Raghavachari, K.; Foresman, J. B.; Ortiz, J. V.; Cui, Q.; Baboul, A. G.; Clifford, S.; Cioslowski, J.; Stefanov, B. B.; Liu, G.; Liashenko, A.; Piskorz, P.; Komaromi, I.; Martin, R. L.; Fox, D. J.; Keith, T.; Al-Laham, M. A.; Peng, C. Y.; Nanayakkara, A.; Challacombe, M.; Gill, P. M. W.; Johnson, B.; Chen, W.; Wong, M. W.; Gonzalez, C.; Pople, J. A. *Gaussian 03*, revision C.02; Gaussian, Inc.: Wallingford, CT, 2004.
(80) Jorgensen, W. L.; Swenson, C. J. *J. Am. Chem. Soc.* **1985**, *107*, 569.
(81) Marcus, Y. *Introduction to Liquid-State Chemistry*; Wiley: New York, 1977.
(82) Kubo, R.; Toda, M.; Hashitsume, N. *Statistical Physics II, Non-equilibrium Statistical Mechanics*; Springer: Berlin, Germany, 1985.
(83) The correlation time is often defined as the integral of $C_L(t)/C_L(0)$. Approximating the behavior of this function around $t \cong 0$ as $\exp[-(u_2/2)t^2] + O(t^4)$, we obtain $\tau_C = (\pi/2u_2)^{1/2} \cong 1.25\tau_f$ as the correlation time.
(84) Kubo, R. *Adv. Chem. Phys.* **1969**, *15*, 101.
(85) As usual, imaginary frequencies are plotted in the negative frequency region.